PERGAMON

International Journal of Solids and Structures 38 (2001) 3853–3875

INTERNATIONAL JOURNAL OF SOLIDS and STRUCTURES

www.elsevier.com/locate/ijsolstr

Higher-order asymptotic crack-tip fields in a power-law creeping material

Y.J. Chao *, X.K. Zhu, L. Zhang

Department of Mechanical Engineering, University of South Carolina, Columbia, SC 29208, USA

Received 26 May 1999

Abstract

The higher-order asymptotic crack-tip fields are considered for a mode-I crack in a power-law creeping material under the plane strain conditions. Based on the three-term solution of Yang et al. (1993) and Chao et al. (1994) for hardening materials, this paper develops a three-term solution near a crack tip in creeping materials only with two parameters: $C(t)$-integral and a constraint parameter $A_2(t)$. This solution is then discussed for conditions of small-scale creep, transient creep and extensive creep. In addition, detailed finite element analysis is performed for four specimens, namely, single-edge notched tension, three point bend, center-cracked panel and compact tension. Good agreement, in both angular and radial stresses, with finite element results confirms that the three-term asymptotic solution is universally valid for specimens possessing various crack-tip constraints and from small-scale creep to extensive creep. This statement is especially true for shallow cracked (or low constraint) specimens, where the dominant region for the HHR-type singularity does not practically exit. © 2001 Elsevier Science Ltd. All rights reserved.

Keywords: Asymptotic analysis; Crack-tip field; Three-term solution; Creeping material; Plane strain

1. Introduction

Accurate description of crack-tip stress and deformation fields is the foundation to establish a reasonable macroscopic fracture criterion and predict the failure of flawed structures. Recently, the research on the higher-order asymptotic crack-tip fields for elastic–plastic materials has received extensive attention. Since the HHR singularity field (Hutchinson, 1968; Rice and Rosengren, 1968) with a single parameter J-integral is not sufficient to characterize the mechanics fields near a crack tip, two-term or multiple-term asymptotic crack-tip fields are presented for power-law hardening materials to study the crack-tip constraint effects. The representatives of which are J–T approach proposed by Betegon and Hancock (1991), J–Q approach by O'Dowd and Shih (1991) and J–A_2 approach by Yang et al. (1993) and Chao et al. (1994). Chao and Zhu (1998), and Zhu and Chao (1999) have given a detailed review about these approaches and concluded that

* Corresponding author. Fax: +1-803-7777-0106.
E-mail address: chao@sc.edu (Y.J. Chao).

0020-7683/01/$ - see front matter © 2001 Elsevier Science Ltd. All rights reserved.
PII: S0020-7683(00)00255-9

the three-term asymptotic solution only with two parameters J and A_2 can describe the crack-tip fields for different cracked specimens from small-scale yielding to large-scale yielding with sufficient accuracy.

The interest in the current paper is to reveal the asymptotic results that can accurately characterize the mechanics fields near a crack tip in creeping materials. Structural failure due to creep fracture at high temperature has drawn much attention over the last two decades. Analytical work was first conducted independently by Riedel and Rice (1980), Riedel (1981) and Ohji et al. (1979) to develop a theoretical basis for the crack-tip stress and deformation fields for plane strain mode-I stationary cracks in power-law creeping materials. Both small-scale creep and extensive creep conditions were considered and the results show that the singular creep crack-tip field is of HRR type with the path-independent integral $C(t)$. Ehlers and Riedel (1981) developed a finite element program to analyze the deformation of a creeping body that contains a stationary mode-I crack. They examined the validity of the approximation involved in the analytical short-time solution and investigated the transient behavior of a compact tension (CT) specimen from small-scale creep to extensive creep. Bassani and McClintock (1981) obtained plane strain numerical solutions for the power-law creep relaxation of crack-tip stresses subsequent to an initial elastic response. It is found that the elastic stress intensity factor K_I and the path-independent C^*-integral are the relevant loading parameters corresponding to short-time and long-time creep, respectively. Li et al. (1988) performed finite element analysis for a crack embedded in an infinite plate to study the dominance of the HRR-type field for a stationary mode-I crack in an elastic-power-law creeping solid under the plain strain conditions. These analyses show that

(a) HRR-type singularity field dominates over a region that is about one-fifth the extent of the creep zone within the transient time.
(b) The time dependence of the amplitude $C(t)$ of the near-tip field is in good agreement with the analysis of Riedel and Rice (1980) and Ohji et al. (1979).
(c) Finite deformation effects dominate over a size scale of the order of the crack tip opening displacement as in the case for rate independent solids.
(d) It was anticipated that under extensive creep conditions, the size of the zone of C^* dominance is strongly dependent on the relative amount of bending to tension around the ligament. If the ligament is subject to primarily tension, the zone of C^* dominance is substantially smaller.

More recently, Yang et al. (1996) carried out detailed finite element analysis for a single-edge notched tension (SENT) in a power-law creeping superalloy material, and studied the HRR-type crack-tip stress and strain fields under both the plane stress and plane strain conditions. Their results indicated that the size of the stress-based HRR-type dominant zone is only a fraction of the creep zone under the plane stress conditions, and is very small (especially along the crack extending line) compared to the creep zone size under the plane strain conditions. Furthermore, the dominance of the singular strain fields is atleast two orders of magnitude smaller than the corresponding stress dominance zones. As such, the use of experimental measurement of surface displacement and/or strain data for the observation of HRR-type fields may not be possible, unless modifications to the existing HRR-type theory are made.

To take the crack-tip constraint effect into account, Shih et al. (1993) extended the J–Q approach (O'Dowd and Shih, 1991) for elastic–plastic materials to creep crack growth, and presented an approximate two-term solution with the parameters $C(t)$ and $Q(t)$. Sharma et al. (1995) compared C^*–Q^* two-term solution under the steady state creep with the finite element results for a shallow SENT specimen having $a/W = 0.05$ in elastic power-law creeping materials. As a result, it is found that the two-term solution provides a more accurate description of the spatial and temporal variations of the crack tip stresses in the creeping materials, whereas the region of dominance of the HRR-type field is essentially zero.

In the J–Q approach, O'Dowd and Shih (1991) argued that the parameter Q is a distance-independent hydrostatic stress ahead of the crack tip. However, the numerical results of Sharma et al. (1995) indicate

that the parameter Q is a hydraulic stress only under the small-scale yielding conditions, and not a hydraulic stress, under the large-scale yielding conditions. Nikishkov et al. (1995b) pointed out that the magnitude of Q is dependent of the distance from the crack tip. On the other hand, Chao and Zhu (1998) revealed that the parameter A_2 is based on rigorous asymptotic solutions and is nearly independent of its position from the crack tip and is valid from small-scale yielding to large-scale yielding. As such, the J–A_2 approach is a more reasonable choice for the characterization of the crack-tip fields. Based on this argument, this paper extends the J–A_2 three-term solution of Yang et al. (1993) and Chao et al. (1994) for elastic–plastic hardening materials to a three-term near-tip solution for a plane strain mode-I crack in power-law creeping materials with only two parameters: $C(t)$-integral and a constraint parameter $A_2(t)$.

To assess the validity of the three-term asymptotic solution for various specimens from small-scale creep to extensive creep, detailed finite element analysis is conducted for four typical fracture test specimens: SENT, three point bend (TPB), center-cracked panel (CCP) and compact tension (CT). Good agreement with finite element results confirms that the three-term asymptotic solution is universally valid for these specimens at different creeping stages and is especially good for low constraint specimen, where the HHR-type singularity field loses the dominant region.

2. Asymptotic crack-tip fields in a creeping material

Our attention in this work is focused on two-dimensional mode-I stationary crack problems under the plane strain conditions. The material deformation behavior is described by elastic-nonlinear viscous constitutive relation according to the Norton power-law creep relation (Nortan (1929)). Under uniaxial tension, the total strain rate is related to the stress by

$$\dot{\varepsilon} = \frac{\dot{\sigma}}{E} + \dot{\varepsilon}_0 \left(\frac{\sigma}{\sigma_0} \right)^n, \tag{1}$$

where E is Young's modulus, σ_0 is a reference stress, $\dot{\varepsilon}_0$ is a reference creep strain rate and n is the creep exponent. (Note that a combined constant $B = \dot{\varepsilon}_0/\sigma_0^n$ is often used).

Under multi-axial stress states, based on the J_2 deformation theory of plasticity, the extension of the uniaxial creep relation (1) can be written as

$$\dot{\varepsilon}_{ij} = \frac{1+\nu}{E}\dot{S}_{ij} + \frac{1-2\nu}{3E}\dot{\sigma}_{kk}\delta_{ij} + \frac{3}{2}\dot{\varepsilon}_0 \left(\frac{\sigma_e}{\sigma_0} \right)^{n-1} \frac{S_{ij}}{\sigma_0}, \tag{2}$$

where ν is the Poisson ratio, and δ_{ij} is the Kronecker delta. A dot over a quantity denotes a time differentiation. $\dot{\varepsilon}_{ij}$ are the components of the strain rate tensor, σ_{ij} are the components of the stress tensor, S_{ij} are the components of the deviatoric stress tensor and $S_{ij} = \sigma_{ij} - \sigma_{kk}\delta_{ij}/3$. σ_e is the Mises effective stress defined by $\sigma_e = ((3/2)S_{ij}S_{ij})^{1/2}$. Typically, the material constants E, ν, n, σ_0, $\dot{\varepsilon}_0$ or B are obtained experimentally from uniaxial tests at the temperature of interest.

2.1. HRR-type leading-term singularity field

It is noted that in the constitutive relations (1) and (2) for elastic-nonlinear-viscous materials, the total strain rate is comprised of elastic strain and creep strain rate. If there is a singularity crack-tip field and the instantaneous response of the material is elastic under sudden applied loading, then at time $t = 0$, the elastic singularity fields prevail at the crack tip. Later, after the load application ($t > 0$) and at distances sufficiently close to the crack tip, the creep strain rate is much larger than the elastic-strain rate and controls

the crack-tip fields ($n > 1$). Accordingly, the material constitutive behaviors Eqs. (1) and (2) become approximate power-law creep relationships.

Hoff (1954) reckoned that if the displacements and strains in elastic–plastic materials are respectively replaced by displacement- and strain-rates in creeping materials in all basic field equations, then the solution constructions are similar for two kinds of materials. Using the Hoff analogy to contrast the power-law creep relation with the power-law hardening relation, Riedel and Rice (1980) and Ohji et al. (1979) presented the HRR-type singularity field (Hutchinson, 1968; Rice and Rosengren, 1968) for power-law creep materials as follows:

$$\begin{aligned}
\sigma_{ij} &= \sigma_0 \left(\frac{C(t)}{\dot{\varepsilon}_0 \sigma_0 I_n r} \right)^{1/(n+1)} \tilde{\sigma}_{ij}(\theta), \\
\dot{\varepsilon}_{ij} &= \dot{\varepsilon}_0 \left(\frac{C(t)}{\dot{\varepsilon}_0 \sigma_0 I_n r} \right)^{n/(n+1)} \tilde{\varepsilon}_{ij}(\theta), \\
\dot{u}_i &= \dot{\varepsilon}_0 r \left(\frac{C(t)}{\dot{\varepsilon}_0 \sigma_0 I_n r} \right)^{n/(n+1)} \tilde{u}_i(\theta),
\end{aligned} \tag{3}$$

where r and θ are polar coordinates centered at the crack tip. The dimensionless constant I_n and the θ-variation functions of the suitably normalized functions $\tilde{\sigma}_{ij}$, $\tilde{\varepsilon}_{ij}$ and $\tilde{u}_i$ depend only on the creep exponent n. These functions have been tabulated in Shih (1983) or Chao and Zhang (1997). The amplitude factor $C(t)$, which depends upon the applied time, magnitude of the remote loading, crack configuration and material properties, is defined as (Bassani and McClintock (1981))

$$C(t) = \int_{\Gamma} \left(\frac{n}{n+1} \sigma_{ij} \dot{\varepsilon}_{ij} n_1 - \sigma_{ij} n_j \dot{u}_{i,1} \right) \mathrm{d}s, \tag{4}$$

where Γ is a vanishingly small, clockwise contour surrounding the crack tip, n_i is the unit outward normal to Γ, $\mathrm{d}s$ is the arc length along Γ and $\dot{u}_{i,1}$ is the displacement gradient rate. It is clear that $C(t)$-integral characterizes the intensity of the near-tip fields in elastic-nonlinear-viscous materials in precisely the same manner as the J-integral does the near-tip fields in rate-independent elastic–plastic materials. Moreover, the $C(t)$-integral is path-independent under steady-state creep conditions.

2.2. $C(t)$–$A_2(t)$ three-term asymptotic solution

As pointed out previously that the HRR-type one-term singularity field (3) generally dominates in a very small region or does not exist near a crack tip for a real specimen. Hence, higher-order asymptotic crack-tip fields are useful for characterizing the mechanics fields near a crack tip in creeping materials. Following the procedure for obtaining the three-term asymptotic solutions for elastic–plastic materials, e.g. Yang et al. (1993), Chao et al. (1994) and Nikishkov (1995a), a three-term asymptotic solution for creeping materials is reported here.

It is assumed that the stress components near a crack tip ($r \to 0$) are separable and can be expressed as a series as

$$\frac{\sigma_{ij}(r,\theta;t)}{\sigma_0} = A_1(t) \left[\bar{r}^{s_1} \tilde{\sigma}_{ij}^{(1)}(\theta) + A_2(t) \bar{r}^{s_2} \tilde{\sigma}_{ij}^{(2)}(\theta) + A_3(t) \bar{r}^{s_3} \tilde{\sigma}_{ij}^{(3)}(\theta) + \cdots \right], \tag{5}$$

where the index 1, 2, 3 correspond to the first-order, second-order and third-order fields, respectively. A_1, A_2, A_3 are undetermined time-dependent constants, s_1, s_2, s_3 are the exponent of stress functions and $s_1 < s_2 < s_3 < \cdots$, $\bar{r} = r/L$, L is a characteristic length. In the polar coordinate system, the equilibrium equations have the following form:

$$\begin{aligned}&\sigma_{rr,r}+\frac{1}{r}\sigma_{r\theta,\theta}+\frac{1}{r}(\sigma_{rr}-\sigma_{\theta\theta})=0,\\&\sigma_{r\theta,r}+\frac{1}{r}\sigma_{\theta\theta,\theta}+\frac{2}{r}\sigma_{r\theta}=0,\end{aligned}\tag{6}$$

where comma denotes a partial derivative with respect to the variable after the comma. Substitution of Eq. (5) into Eq. (6) yields the relationships among the angular stress functions

$$\left.\begin{aligned}&(s_m+1)\sigma_{rr}^{(m)}-\sigma_{\theta\theta}^{(m)}+\sigma_{r\theta,\theta}^{(m)}=0\\&\sigma_{\theta,\theta}^{(m)}+(s_m+2)\sigma_{r\theta}^{(m)}=0\end{aligned}\qquad(m=1,2,3)\right\}.\tag{7}$$

Based on the definition of the Mises effective stress σ_e and the stress asymptotic expansion (5), one has

$$\begin{aligned}\left(\frac{\sigma_e}{\sigma_0}\right)^{n-1}=\Big\{&A_1^2\bar{r}^{2s_1}(\tilde{\sigma}_e^{(11)}(\theta))^2[1+2A_2\bar{r}^{s_2-s_1}\tilde{\sigma}_e^{(12)}(\theta)+2A_3\bar{r}^{s_3-s_1}\tilde{\sigma}_e^{(13)}(\theta)+2A_2^2\bar{r}^{2s_2-2s_1}\tilde{\sigma}_e^{(22)}(\theta)\\&+2A_2A_3\bar{r}^{s_2+s_3-2s_1}\tilde{\sigma}_e^{(23)}(\theta)+2A_3^2\bar{r}^{2s_3-2s_1}\tilde{\sigma}_e^{(33)}(\theta)+\cdots]\Big\}^{(n-1/2)},\end{aligned}\tag{8}$$

where

$$\tilde{\sigma}_e^{(11)}=\left(\tfrac{3}{2}\tilde{S}_{ij}^{(1)}\tilde{S}_{ij}^{(1)}\right)^{1/2},\tag{9a}$$

$$\tilde{\sigma}_e^{(kl)}=\frac{3}{2}\frac{\tilde{S}_{ij}^{(k)}\tilde{S}_{ij}^{(l)}}{(\tilde{\sigma}_e^{(11)})^2}\qquad(k,l=1,2,3\ \text{and}\ k+l\neq 2),\tag{9b}$$

$$\tilde{S}_{ij}^{(k)}=\tilde{\sigma}_{ij}^{(k)}-\tilde{\sigma}_{kk}^{(k)}\delta_{ij}/3.\tag{9c}$$

Substituting the stress expansion (5) and the effective stress expansion (8) into the constitutive Eq. (2), one obtains the asymptotic expansion of strain rate components

$$\begin{aligned}\frac{\dot{\varepsilon}_{ij}}{\dot{\varepsilon}_0}=&A_1^n[\bar{r}^{ns_1}\tilde{\varepsilon}_{ij}^{(1)}(\theta)+A_2\bar{r}^{s_1(n-1)+s_2}\tilde{\varepsilon}_{ij}^{(2)}(\theta)+A_3\bar{r}^{s_1(n-1)+s_3}\tilde{\varepsilon}_{ij}^{(3)}(\theta)+A_2^2\bar{r}^{s_1(n-2)+2s_2}\tilde{\xi}_{ij}^{(1)}(\theta)]\\&+A_1[\bar{r}^{s_1}\tilde{\eta}_{ij}^{(1)}(\theta)+A_2\bar{r}^{s_2}\tilde{\eta}_{ij}^{(2)}(\theta)+A_3\bar{r}^{s_3}\tilde{\eta}_{ij}^{(3)}(\theta)]+\cdots,\end{aligned}\tag{10}$$

where

$$\tilde{\varepsilon}_{ij}^{(1)}=\tfrac{3}{2}\tilde{\sigma}_e^{(11)n-1}\tilde{S}_{ij}^{(1)},\tag{11a}$$

$$\tilde{\varepsilon}_{ij}^{(2)}=\tfrac{3}{2}\tilde{\sigma}_e^{(11)n-1}[\tilde{S}_{ij}^{(2)}+(n-1)\tilde{\sigma}_e^{(12)}\tilde{S}_{ij}^{(1)}],\tag{11b}$$

$$\tilde{\varepsilon}_{ij}^{(3)}=\tfrac{3}{2}\tilde{\sigma}_e^{(11)n-1}\left[\tilde{S}_{ij}^{(3)}+(n-1)\tilde{\sigma}_e^{(13)}\tilde{S}_{ij}^{(1)}\right],\tag{11c}$$

$$\tilde{\xi}_{ij}^{(1)}=\tfrac{3}{2}\tilde{\sigma}_e^{(11)n-1}(n-1)\left\{\tilde{\sigma}_e^{(12)}\tilde{S}_{ij}^{(2)}+\tfrac{1}{2}[\tilde{\sigma}_e^{(22)}+(n-3)(\tilde{\sigma}_e^{(12)})^2]S_{ij}^{(1)}\right\},\tag{11d}$$

$$\tilde{\eta}_{ij}^{(m)}=\frac{1+v}{E\dot{\varepsilon}_0}\dot{\tilde{S}}_{ij}^{(m)}+\frac{1-2v}{3E\dot{\varepsilon}_0}\dot{\tilde{\sigma}}_{kk}^{(m)}\delta_{ij}\qquad(m=1,2,3).\tag{11e}$$

The geometric relations between strain rate and displacement rate components in the polar coordinate system can be written as

$$\begin{aligned}\dot{\varepsilon}_{rr} &= \dot{u}_{r,r},\\ \dot{\varepsilon}_{\theta\theta} &= \frac{1}{r}(\dot{u}_r + \dot{u}_{\theta,\theta}),\\ \dot{\varepsilon}_{r\theta} &= \frac{1}{2r}(\dot{u}_{r,\theta} + r\dot{u}_{\theta,r} - \dot{u}_\theta).\end{aligned} \tag{12}$$

From Eqs. (10) and (12), one can obtain the asymptotic expansions of displacement rate components

$$\frac{\dot{u}_i}{\dot{\varepsilon}_0 L} = A_1^n[\bar{r}^{ns_1+1}\tilde{u}_i^{(1)}(\theta) + A_2\bar{r}^{s_1(n-1)+s_2+1}\tilde{u}_i^{(2)}(\theta) + A_3 r^{s_1(n-1)+s_3+1}\tilde{u}_i^{(3)}(\theta)] + \cdots, \tag{13}$$

where

$$\begin{cases}\tilde{u}_r^{(1)} = \frac{\tilde{\varepsilon}_{rr}^{(1)}}{ns_1+1} = \tilde{\varepsilon}_{\theta\theta}^{(1)} - \tilde{u}_{\theta,\theta}^{(1)},\\ \tilde{u}_\theta^{(1)} = \frac{2\tilde{\varepsilon}_{r\theta}^{(1)} - \tilde{u}_{r,\theta}^{(1)}}{ns_1},\end{cases} \tag{14a}$$

$$\begin{cases}\tilde{u}_r^{(2)} = \frac{\tilde{\varepsilon}_{rr}^{(2)}}{(n-1)s_1+s_2+1} = \tilde{\varepsilon}_{\theta\theta}^{(2)} - \tilde{u}_{\theta,\theta}^{(2)},\\ \tilde{u}_\theta^{(2)} = \frac{2\tilde{\varepsilon}_{r\theta}^{(2)} - \tilde{u}_{r,\theta}^{(2)}}{(n-1)s_1+s_2},\end{cases} \tag{14b}$$

$$\begin{cases}\tilde{u}_r^{(3)} = \frac{\tilde{\varepsilon}_{rr}^{(3)} + \tilde{\xi}_{rr}^{(1)}}{(n-1)s_1+s_3+1} = \tilde{\varepsilon}_{\theta\theta}^{(3)} + \tilde{\xi}_{\theta\theta}^{(1)} - \tilde{u}_{\theta,\theta}^{(3)},\\ \tilde{u}_\theta^{(3)} = \frac{2\tilde{\varepsilon}_{r\theta}^{(3)} + 2\tilde{\xi}_{r\theta}^{(1)} - \tilde{u}_{r,\theta}^{(3)}}{(n-1)s_1+s_3}.\end{cases} \tag{14c}$$

Eqs. (7) and (11) and (14) are the final governing equations for the first-order, second-order and third-order asymptotic fields. *They are exactly the same as those given by Nikishkov* (1995) *for power-law hardening materials*. If the Airy stress function was used, one would obtain the governing equations exactly as those reported by Yang et al. (1993). Accordingly, the solution properties and the angular functions of stress, strain and displacement rate are the same as those for power-law hardening materials. Several conclusions can thus be summarized as follows:

(a) The first-order asymptotic field is the HRR-type singularity field, and thus

$$A_1(t) = \left(\frac{C(t)}{\sigma_0\dot{\varepsilon}_0 I_n L}\right)^{1/(n+1)}, \qquad s_1 = -\frac{1}{n+1}. \tag{15}$$

(b) The amplitudes of the second-order and third-order fields are not independent of each other and have a simple relationship

$$A_3 = A_2^2. \tag{16}$$

(c) For the creep exponent $n \geqslant 3$, the stress exponents are related by

$$s_3 = 2s_2 - s_1. \tag{17}$$

(d) From moderate to low creeping materials, i.e. $n \geqslant 3$, three-term solution with $C(t)$–$A_2(t)$ as the two parameters is the pure power-law creep solution. The elastic strain rate has no role on the crack-tip fields.

Therefore, from Eqs. (5), (10), (13), and (15)–(17), $C(t)$–$A_2(t)$ three-term solutions of stress, strain and displacement rate for power-law creeping materials can be written as

$$\begin{aligned}
\frac{\sigma_{ij}(r,\theta;t)}{\sigma_0} &= A_1(t)\left[\bar{r}^{s_1}\tilde{\sigma}_{ij}^{(1)}(\theta) + A_2(t)\bar{r}^{s_2}\tilde{\sigma}_{ij}^{(2)}(\theta) + A_2^2(t)\bar{r}^{s_3}\tilde{\sigma}_{ij}^{(3)}(\theta)\right],\\
\frac{\dot{\varepsilon}_{ij}(r,\theta;t)}{\dot{\varepsilon}_0} &= A_1^n(t)\left[\bar{r}^{ns_1}\tilde{\varepsilon}_{ij}^{(1)}(\theta) + A_2(t)\bar{r}^{(n-1)s_1+s_2}\tilde{\varepsilon}_{ij}^{(2)}(\theta) + A_2^2(t)\bar{r}^{(n-1)s_1+s_3}\tilde{\varepsilon}_{ij}^{*(3)}(\theta)\right],\\
\frac{\dot{u}_i(r,\theta;t)}{\dot{\varepsilon}_0 L} &= A_1^n(t)\left[\bar{r}^{ns_1+1}\tilde{u}_i^{(1)}(\theta) + A_2(t)\bar{r}^{s_1(n-1)+s_2+1}\tilde{u}_i^{(2)}(\theta) + A_2^2(t)r^{s_1(n-1)+s_3+1}\tilde{u}_i^{(3)}(\theta)\right],
\end{aligned} \tag{18}$$

where $A_1(t)$ is defined by Eq. (15), $A_2(t)$ is an undetermined parameter and may be related to the loading condition, creep time and specimen geometry, $\bar{r} = r/L$ and L is a crack characteristic length which can be taken as crack depth, specimen width, unit 1 cm and so on. The stress exponents s_1, s_2, s_3, the integral constant I_n, and the dimensionless angular functions $\tilde{\sigma}_{ij}^{(m)}$, $\tilde{\varepsilon}_{ij}^{(m)}$, $\tilde{\varepsilon}_{ij}^{*(m)}(m = 1, 2, 3;\ \tilde{\varepsilon}_{ij}^{*(3)} = \tilde{\varepsilon}_{ij}^{(3)} + \tilde{\xi}_{ij}^{(1)})$ are tabulated by Chao and Zhang (1997). It can be easily observed that when $A_2 = 0$, the three-term solution (18) reduces to the leading-term HRR singularity field (3).

It is noted that the parameter $A_2(t)$ cannot be determined in the asymptotic analysis. It can be determined by matching the three-term stress solutions in Eq. (18) with known crack-tip fields, such as finite element results. A few methods have been proposed for this purpose, e.g. *the point-matching technique* of Chao et al. (1994), *the least square approach* of Nikishkov et al. (1995b) and *the weight function approach* of Chao and Zhu (2000). In this paper, the specimen width W is used as the characteristic length L, the stress components σ_{rr} and $\sigma_{\theta\theta}$ at $r/a = 0.01$–0.1, $\theta = 0°$ and $45°$ are used to determine an average value of $A_2(t)$ by matching the three-term solution in the first part of Eq. (18) with finite element results.

If we use the creep material constant $B = \dot{\varepsilon}_0/\sigma_0^n$, the $C(t)$–$A_2(t)$ three-term solution (18) can be written as

$$\begin{aligned}
\sigma_{ij}(r,\theta;t) &= \bar{A}_1(t)\left[\bar{r}^{s_1}\tilde{\sigma}_{ij}^{(1)}(\theta) + A_2(t)\bar{r}^{s_2}\tilde{\sigma}_{ij}^{(2)}(\theta) + A_2^2(t)\bar{r}^{s_3}\tilde{\sigma}_{ij}^{(3)}(\theta)\right],\\
\dot{\varepsilon}_{ij}(r,\theta;t) &= B\bar{A}_1^n(t)\left[\bar{r}^{ns_1}\tilde{\varepsilon}_{ij}^{(1)}(\theta) + A_2(t)\bar{r}^{(n-1)s_1+s_2}\tilde{\varepsilon}_{ij}^{(2)}(\theta) + A_2^2(t)\bar{r}^{(n-1)s_1+s_3}\tilde{\varepsilon}_{ij}^{*(3)}(\theta)\right],\\
\dot{u}_i(r,\theta;t) &= BL\bar{A}_1^n(t)\left[\bar{r}^{ns_1+1}\tilde{u}_i^{(1)}(\theta) + A_2(t)\bar{r}^{s_1(n-1)+s_2+1}\tilde{u}_i^{(2)}(\theta) + A_2^3(t)r^{s_1(n-1)+s_3+1}\tilde{u}_i^{(3)}(\theta)\right],
\end{aligned} \tag{19}$$

where

$$\bar{A}_1(t) = \left(\frac{C(t)}{BI_nL}\right)^{(1/n+1)}. \tag{20}$$

Note that, if we make an assumption a priori that the deformation near a crack tip is controlled by the creep and the elastic strains can be neglected, the material considered becomes a pure power-law creeping material. Using the Hoff analogy (Hoff, 1954), the $C(t)$–$A_2(t)$ three-term solution (18) can also be obtained directly from the J–A_2 three-term solution by Yang et al. (1993) and Chao et al. (1994) for power-law hardening materials when J is replaced by $C(t)$ and $\alpha\varepsilon_0$ is replaced by $\dot{\varepsilon}_0$.

2.3. Expressions of $C(t)$ under different creep conditions

The amplitude $C(t)$-integral in the three-term solution (18) is defined in Eq. (4) and depends generally on the creep time, magnitude of the applied loading, crack geometry and material properties. It is clear that $C(t)$-integral characterizes the intensity of the crack-tip asymptotic fields (18) in elastic-nonlinear-viscous materials. Thus, an accurate, yet simple, method for determining $C(t)$ is important. Due to the complexities involved in evaluating $C(t)$ from Eq. (4), approximate solutions of $C(t)$ have been developed at different creeping stages.

2.3.1. Small-scale creep

A small-scale creep is the short-time creep. At short times, after load application, the elastic strains are much greater than the creep strains everywhere except in a small region at the crack tip, which is referred to as 'creep zone'. Riedel and Rice (1980) and Ohji et al. (1979) showed that the small-scale creep fields are self-similar and that there is creep zone, where the spatial dependence of the stress and creep strain are precisely given by the asymptotic fields. In the outer region of the creep zone, the linear elastic crack-tip field still dominates. As a result, they obtained the simple expression

$$C(t) = \frac{K_I^2(1-\nu^2)/E}{(n+1)t}, \tag{21}$$

where K_I is the stress intensity factor of a mode-I crack. Eq. (18) or Eq. (19) in conjunction with Eq. (21) is the three-term asymptotic fields under the small-scale creep conditions, which is valid as long as the creep zone is sufficiently small compared with the dimensions of the specimen.

2.3.2. Extensive creep

At later times after the load is applied, the whole specimen creeps extensively and the elastic strain can be neglected compared to creep strain. The deformation of material enters the stage of steady-state creep and the stresses become time-independent ($\dot{\sigma} \to 0$) as $t \to \infty$, if the load is kept constant and finite geometry changes can be neglected. As a consequence, all field quantities become time-independent. In this case, $C(t) \to C^*$, $A_2(t) \to A_2^*$ as $t \to \infty$, where C^* is a path-independent integral. Hence, the three-term asymptotic fields (19) under the steady-state creep can be written as

$$\begin{aligned}
\sigma_{ij}(r,\theta) &= \left(\frac{C^*}{BI_nL}\right)^{(1/n+1)} \left[\bar{r}^{s_1}\tilde{\sigma}_{ij}^{(1)}(\theta) + A_2^*\bar{r}^{s_2}\tilde{\sigma}_{ij}^{(2)}(\theta) + A_2^{*2})\bar{r}^{s_3}\tilde{\sigma}_{ij}^{(3)}(\theta)\right],\\
\dot{\varepsilon}_{ij}(r,\theta) &= B\left(\frac{C^*}{BI_nL}\right)^{(n/n+1)} \left[\bar{r}^{ns_1}\tilde{\varepsilon}_{ij}^{(1)}(\theta) + A_2^*\bar{r}^{(n-1)s_1+s_2}\tilde{\varepsilon}_{ij}^{(2)}(\theta) + A_2^{*2}\bar{r}^{(n-1)s_1+s_3}\tilde{\varepsilon}_{ij}^{*(3)}(\theta)\right],\\
\dot{u}_i(r,\theta) &= BL\left(\frac{C^*}{BI_nL}\right)^{(n/n+1)} \left[\bar{r}^{ns_1+1}\tilde{u}_i^{(1)}(\theta) + A_2^*\bar{r}^{s_1(n-1)+s_2+1}\tilde{u}_i^{(2)}(\theta) + A_2^{*2}(t)r^{s_1(n-1)+s_3+1}\tilde{u}_i^{(3)}(\theta)\right].
\end{aligned} \tag{22}$$

The extensive creep case is completely analogous to the fully plastic state in rate-independence materials. Through the Hoff analogy, the C^*-integral can be obtained from the fully plastic J-integral, if the strains ε_{ij} are replaced by the strain rates $\dot{\varepsilon}_{ij}$, or the material constant $\alpha\varepsilon_0/\sigma_0^n$ is replaced by the creep constant B. Thus, a typical extensive creep solution of C^* can be expressed by Li et al. (1988)

$$C^* = B(W-a)h\left(\frac{a}{W}, n\right)\left(\frac{P\sigma_0}{P_0}\right)^{n+1}, \tag{23}$$

where W is the specimen width, a is the crack depth, h is a dimensionless function of creep exponent n and geometric parameter a/W, and is tabulated in the elastic–plastic handbook (Kumar et al. (1981)). P is the applied load, and P_0 is an appropriate reference load, e.g. the limit load for an equivalent fully plastic body with a yield stress σ_0.

2.3.3. Transition from small-scale creep to extensive creep

The characteristic time t_T for transition from small-scale creep to extensive creep was estimated by Riedel and Rice (1980) and Ohji et al. (1979) and is given as

$$t_T = \frac{K_I^2(1-\nu^2)}{(n+1)EC^*}. \tag{24}$$

It is clear that the transition time t_T depends on the applied load, crack configuration and the elastic and creep properties of materials. For times shorter than t_T, the amplitude $C(t)$ of the crack-tip fields is given by the small-scale result in Eq. (21), whereas for times longer than t_T, the amplitude $C(t)$ is given by the steady state value C^* in Eq. (23). In the interval between small-scale creep and extensive-creep, Ehlers and Riede (1981) suggested the following interpolation formula for $C(t)$:

$$C(t) = C^*(t_T/t + 1). \tag{25}$$

Eq. (18) or Eq. (19) in conjunction with Eq. (25) is the three-term asymptotic fields under the transient creep condition.

3. Numerical results and comparisons

In order to assess the validity of the three-term asymptotic solution (18) or (19) under different creep conditions, detailed finite element analyses were conducted for four typical fracture test specimens as shown in Fig. 1. These specimens are SENT, TPB, CCP and CT. Then the asymptotic solutions are compared with the numerical results. The extent of dominance of the three-term solution under different creep conditions is obtained for the four specimens.

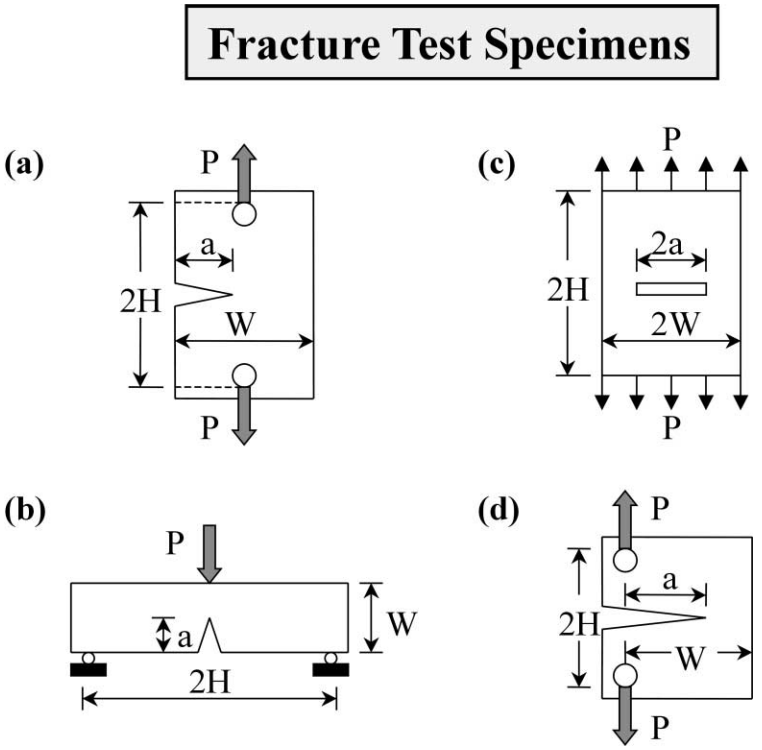

Fig. 1. Specimen geometries: (a) SENT; (b) TPB; (c) CCP; and (d) CT.

3.1. Finite element model

The commercial finite element code, ABAQUS (version 5.7-1), was used to model the stationary cracked specimens under the mode-I plane strain conditions in this work. The numerical model employs the conventional small-strain theory and the material deformation obeys the constitutive relation (2). The material used in this calculation is a superalloy, Inconel 800 H, at 1200°F. The material properties are $E = 22.294$ Mpsi, $\sigma_0 = 60487$ psi, $\nu = 0.33$, $n = 5$, $B = 2.1 \times 10^{-27}$ $(\text{psi})^{-5}/\text{h}$.

Due to the symmetry of specimens, a half of SENT, TPB and CT specimens and a quarter of CCP specimen were modeled. A typical finite element mesh is shown in Fig. 2. The eight-node isoparametric element with reduced integration (element type CPE8R) was used in all the calculations. The mesh consists of 588 eight-node elements and 1873 nodes with 28 rings of elements and 36 elements in each ring for short time creep ($t < t_T$, t_T is the transition time), and 318 elements and 1033 nodes with 14 rings of element and 18 elements in each ring for long time creep ($t \geqslant t_T$). The two cases with different number of elements have approximately the same computation accuracy.

In all calculations, the load is applied instantaneously to the specimens, and then holds constant until steady-state creep conditions are reached. Initial application of the load is assumed to occur so quickly that it involves purely elastic response. $C(t)$-integral and the crack-tip field quantities were computed directly by the ABAQUS.

3.2. Single edge notched tension specimen with $a/W = 0.125$

A SENT specimen with a shallow crack as illustrated in Fig. 1(a) is considered in this section. The specimen has a crack depth of $a/W = 0.125$, width $W = 40$ inch, length $2H = 5W$, and a thickness $b = 40$ in. The remote uniform load is 30,000 psi, which corresponds to an applied concentrated load of $P = 48$ Mlb.

3.2.1. Time-dependence (creep zone, $C(t)$, $A_2(t)$)

Fig. 3 shows the development of the creep zone at the crack tip for the SENT specimen at different time. The creep zone boundary is defined as the region, where the effective creep strain $\bar{\varepsilon}^c$ is equal to the effective elastic strain $\bar{\varepsilon}^e$, that is $\bar{\varepsilon}^c = \bar{\varepsilon}^e$. The size and shape of the creep zone show that the maximum distance of

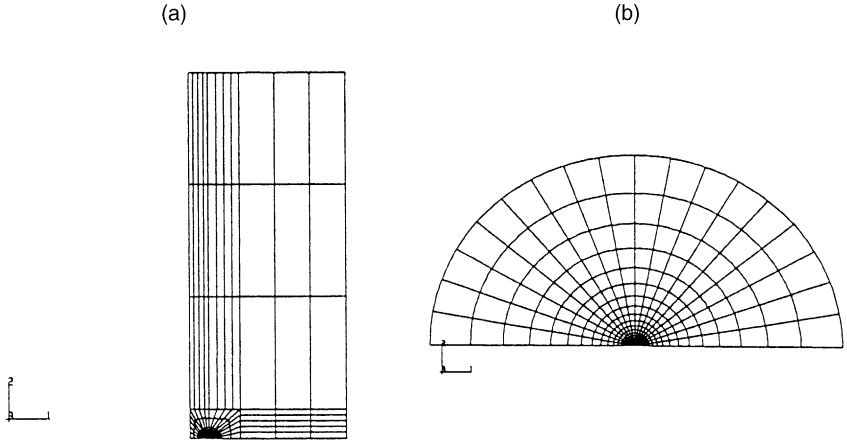

Fig. 2. Finite element mesh for specimen analyzed which comprises of eight-node plane strain isoparametric elements (a) Entire specimen mesh and (b) Crack-tip mesh.

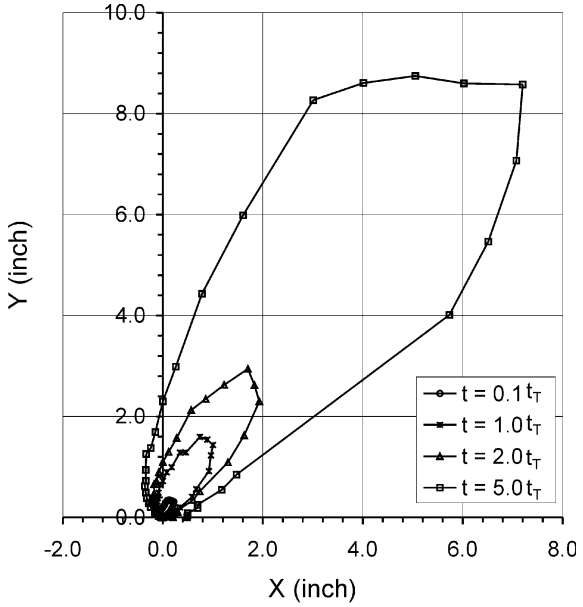

Fig. 3. The size and shape of creep zone for SENT specimen with $a/W = 0.125$ at time $t = 0.1t_T$, $1.0t_T$, 2.0 t_T and 5.0 t_T.

creep zone boundary from the crack tip occurs at about $55° \leqslant \theta \leqslant 65°$ measured from the crack line. The creep zone agrees well in shape as compared with the result obtained by Ehlers and Riedel (1981) for the CT-specimen, Li et al. (1988) for the semi-infinite plate with an edge crack. The maximum extent of the creep zone size at time $t = 0.1t_T$, $t = 1.0t_T$, $t = 2.0t_T$ and $t = 5.0t_T$ are $0.076a$, $0.336a$, $0.68a$ and $2.6a$, respectively, where a is the crack depth. For the whole specimen, the creep strain dominates inside the creep zone, while the elastic strain prevails outside the creep zone.

Fig. 4 shows that the variation of $C(t)$-integral with time for the shallow cracked SENT specimen. The results in this figure are obtained from the finite element analysis (FEA), Riedel and Rice's short time estimation formula (21) and Ehlers and Riedel's approximate interpolation formula (25) for transient time between small-scale creep and extensive creep. For SENT specimens, the steady-state value C^*, e.g. Eq. (23), becomes

$$C^* = B(w-a)(a/w)h_1(a/w,n)(P\sigma_0/P_0)^{n+1}, \tag{26}$$

where the reference load per unit thickness is

$$P_0 = 1.455\eta(w-a)\sigma_0 \tag{27}$$

in which

$$\eta = \left(1 + \left(\frac{a}{w-a}\right)^2\right)^{1/2} - \left(\frac{a}{w-a}\right). \tag{28}$$

For the SENT specimen with $a/W = 1/8$, $h_1 = 11.5$ (Kumar et al. (1981)), thus the C^*-integral for this case is 42.52 psi-in/h from Eqs. (26) and (27). And so the transition time $t_T = 225$ h, which is calculated from Eq. (24). At this transition time, i.e. $t = t_T$, the $C(t)$-integral from the FEA is determined as 90.84 psi-in/h.

It is found that for very short time ($t < 0.06t_T$), the $C(t)$-integral obtained from Eqs. (21) and (25) does not agree with the results from FEA. Their errors compared with FEA are greater than 10%. For short time

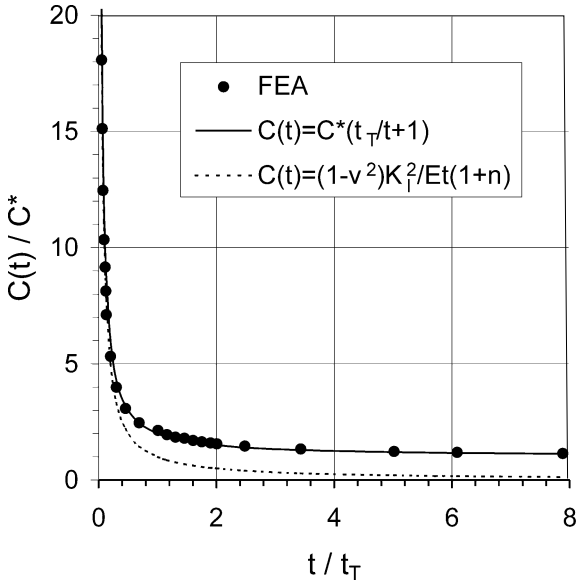

Fig. 4. Variation of $C(t)$-integral with time for SENT specimen with $a/W = 0.125$.

($0.06 \leqslant t_T \leqslant 0.3t_T$), the estimation of the $C(t)$-integral from Eq. (21) agrees very well with FEA results, while for long time ($t > 0.3t_T$), the $C(t)$-integral from interpolation formula (25) is in agreement with the FEA results. At the time about $t = 5t_T$, the $C(t)$-integral approaches the steady-state value $C^* = 42.52$ psi-in/h.

Fig. 5(a) is the temporal variation of the amplitude $A_2(t)$ in the three-term asymptotic solution (18) at different location near the crack tip of the shallow cracked SENT ($r/a = 0.018, 0.04, 0.1$). It is observed that the creep time has certain influence on $A_2(t)$ only in short time $t < t_T$. One can conclude that the amplitude $A_2(t)$ in the three-term asymptotic solution for power-law creeping materials is *approximately* independent of the creep time. On the other hand, the creep time has significant effect on the load parameter $C(t)$-integral as shown in Fig. 4. In fact, most recently Chao and Zhu (2000) has theoretically proved that the value of the constraint parameter A_2 in the J–A_2 three-term solution is independent of the applied loads for power-law hardening materials or under the large-scale yielding conditions. In terms of the Hoff analogy (Hoff, 1954), $A_2(t)$ in the $C(t)$–$A_2(t)$ three-term solution can also be interpreted as a constraint parameter and is independent of the applied loads, including the generalized load-time, for power-law creeping materials or extensive creep. So hereafter, we shall denote $A_2(t)$ in the three-term solution (18) or (19) as A_2.

Fig. 5(b) depicts the variations of amplitude A_2 with the distance from the crack tip at the time $t = t_T$ for the shallow cracked SENT specimen. The value of A_2 is approximately a constant in the region $r/a > 0.03$.

3.2.2. Radial and angular distributions of stress field

In order to demonstrate the validity of the three-term asymptotic solution (19), in this section we report and compare the finite element results, HRR-type fields and the three-term asymptotic solutions. In all figures of this paper, FEA represents the finite element numerical results, HRR denotes the HRR-type singularity field and TTS indicates the C–A_2 three-term solution. To judge the degree of agreement between the FEA results and the asymptotic solutions (HRR-type field or the C–A_2 three-term solution), we adopt the criterion that "good agreement" is defined as when the difference between the FEA results and the asymptotic solutions is within 10 percent of the asymptotic solutions. Fig. 6 shows the radial distributions of stresses for SENT specimens with $a/W = 0.125$ at time $t = 0.1t_T$, position $\theta = 0°$ and $\theta = 45°$. Fig. 7

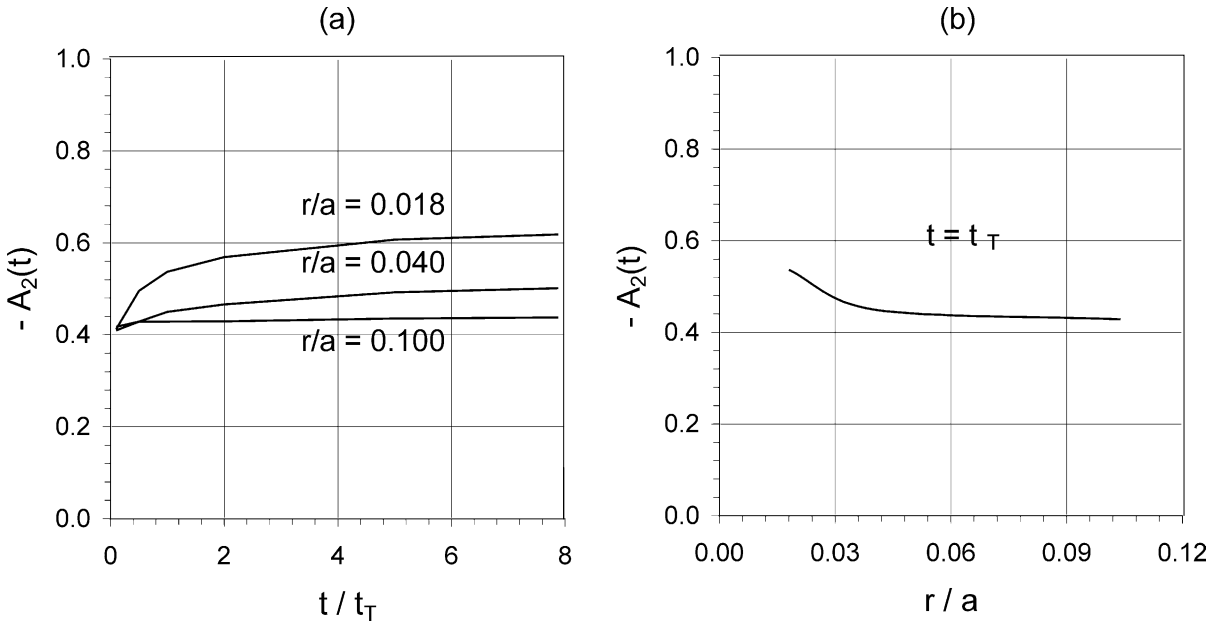

Fig. 5. Variations of amplitude A2 for SENT specimen of $a/W = 0.125$ with (a) time and (b) the distance from crack tip.

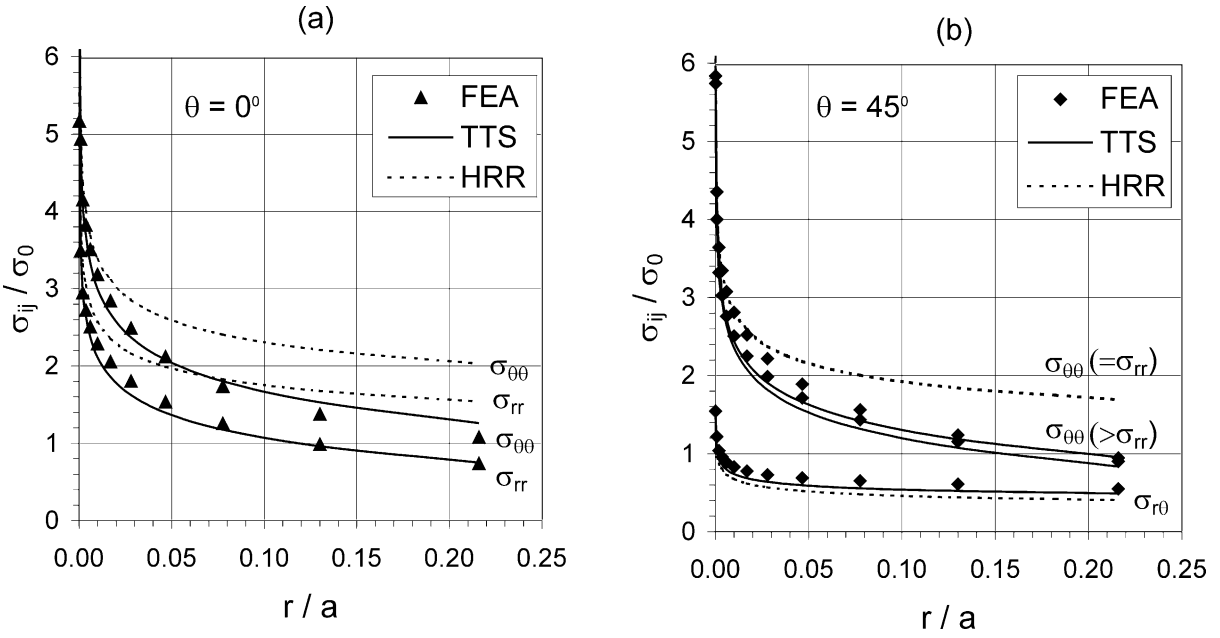

Fig. 6. Radial distributions of stresses at $t = 0.1t_T$ for SENT specimen with $a/W = 0.125$ (a) $\theta = 0°$ and (b) $\theta = 45°$.

shows the angular distributions of the stresses for SENT specimens with $a/W = 0.125$ at time $t = 0.1t_T$, position $r/a = 0.01$ and $r/a = 0.1$. It is observed that in Fig. 7 the three-term solutions of all stress

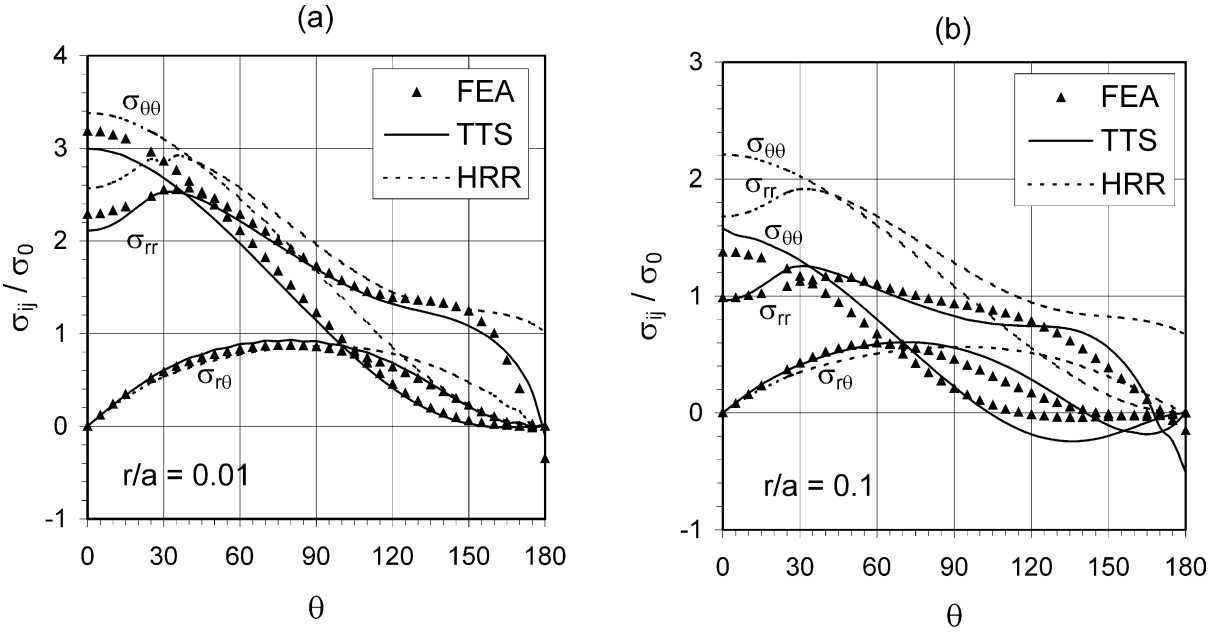

Fig. 7. Angular distributions of stresses at $t = 0.1t_T$ for SENT specimen with $a/W = 0.125$ (a) $r/a = 0.01$ and (b) $r/a = 0.1$.

components σ_{rr}, $\sigma_{\theta\theta}$ and $\sigma_{r\theta}$ match very well with the finite element results, whereas the HRR-type fields are close to the FEA results at $r/a = 0.01$ and deviate significantly from the FEA results at $r/a = 0.1$. In the radial direction, the three-term solutions are in good agreement with the FEA results from crack tip to even beyond $r/a > 0.2$, at both $\theta = 0°$ and $\theta = 45°$, while the dominant region of the HRR-type fields is only within $r/a \leqslant 0.01$. Note that in Fig. 6, $\sigma_{rr} = \sigma_{\theta\theta}$ from the HRR-type field, however, actually $\sigma_{rr} \neq \sigma_{\theta\theta}$ although the difference is small as can be seen from both the FEA results and the three-term solution.

For the SENT specimens with $a/W = 0.125$, at time $t = 1.0t_T$, the radial distributions of the stresses in the direction of $\theta = 0°$ and $\theta = 45°$ are plotted in Fig. 8; the angular distributions of the stresses at the position from the crack tip $r/a = 0.018$ and $r/a = 0.1$ are depicted in Fig. 9. At time $t = 7.8t_T$, the radial distributions of the stresses in the direction of $\theta = 0°$ and $\theta = 45°$ are illustrated in Fig. 10; and the angular distributions of the stresses at the position $r/a = 0.018$ and $r/a = 0.1$ are shown in Fig. 11. Again, all calculated stress components in both angular and radial directions are in good agreement with those from the three-term solutions, but deviated substantially from those of HRR-type fields. In the radial directions of $\theta = 0°$ and $\theta = 45°$, the three-term solutions match well with the FEA results up to $r/a = 0.2$ when $t = 1.0t_T$ and $r/a = 0.1$ when $t = 7.8t_T$. In the circumferential positions of $r/a = 0.018$ and $r/a = 0.1$, all stresses from the three-term solutions are consistent with the calculated stresses over the entire angular sectors except for the sector near to the crack surface of $\theta = 180°$. This is reasonable because the region near the crack surface is in elastic states from FEA, for instance, the zones of $\theta \leqslant 30°$ and $\theta \geqslant 110°$ is outside the creep zone at $t = t_T$ and $r/a = 0.1$, while the three-term solution is pure creep solution and as such cannot match well with the elastic results. In spite of this, the three-term solutions qualitatively coincide with the FEA results, but the HRR-type results cannot. Near the crack surface of $\theta = 180°$, the radial stress σ_{rr} is less than zero from both FEA and TTS, but is more than zero based on the HRR-type field. As a result, the HRR-type field incorrectly characterizes the actual compressible stress state by a tensile stress.

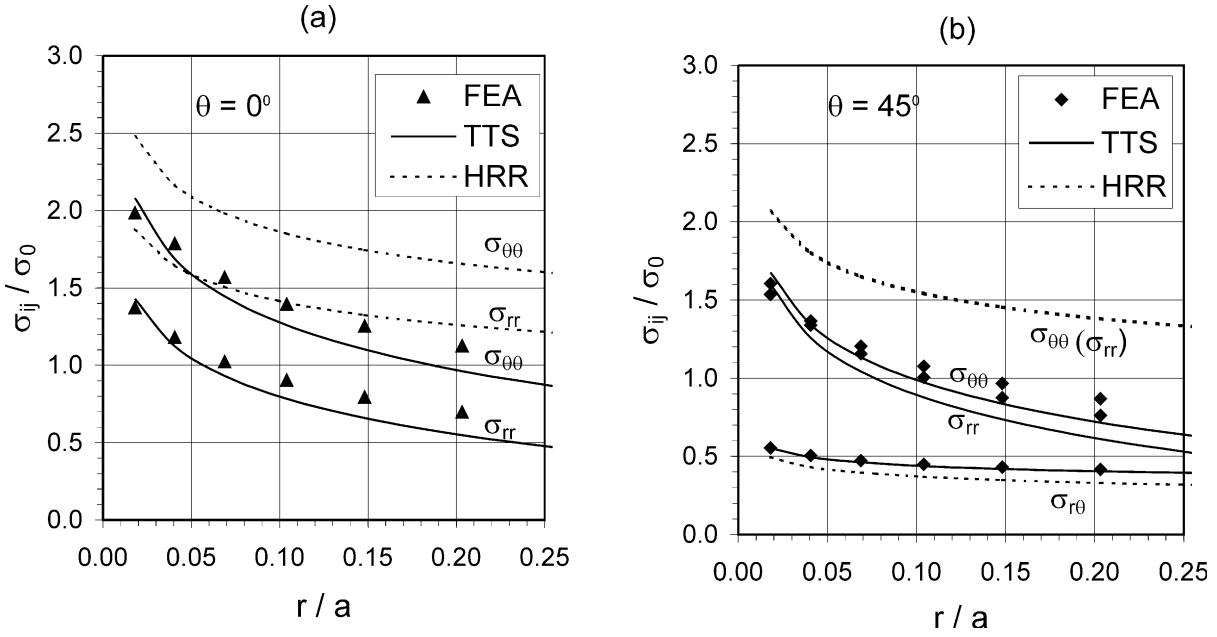

Fig. 8. Radial distributions of stresses at $t = 1t_T$ for SENT specimen with $a/W = 0.125$ (a) $\theta = 0°$ and (b) $\theta = 45°$.

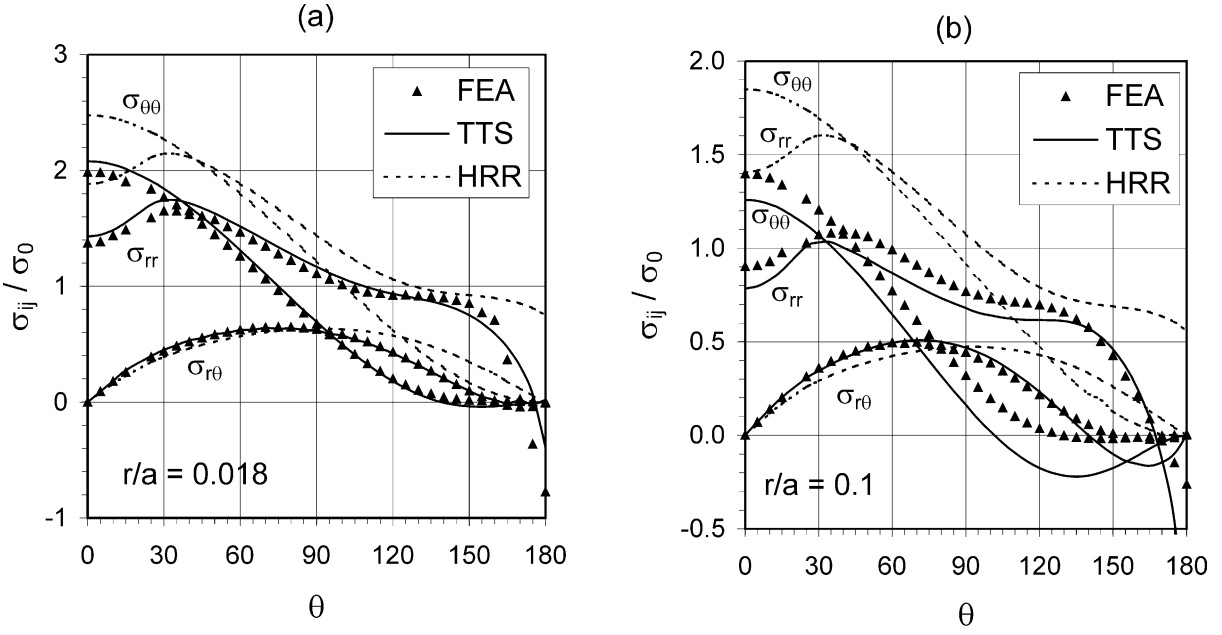

Fig. 9. Angular distributions of stresses at $t = 1t_T$ for SENT specimen with $a/W = 0.125$ (a) $r/a = 0.018$ and (b) $r/a = 0.1$.

In summary, for the shallow cracked SENT specimens from small-scale creep (i.e. time $t = 0.1t_T$) to extensive creep (i.e. time $t = 7.8t_T$), the three-term solution compares well with the finite element results

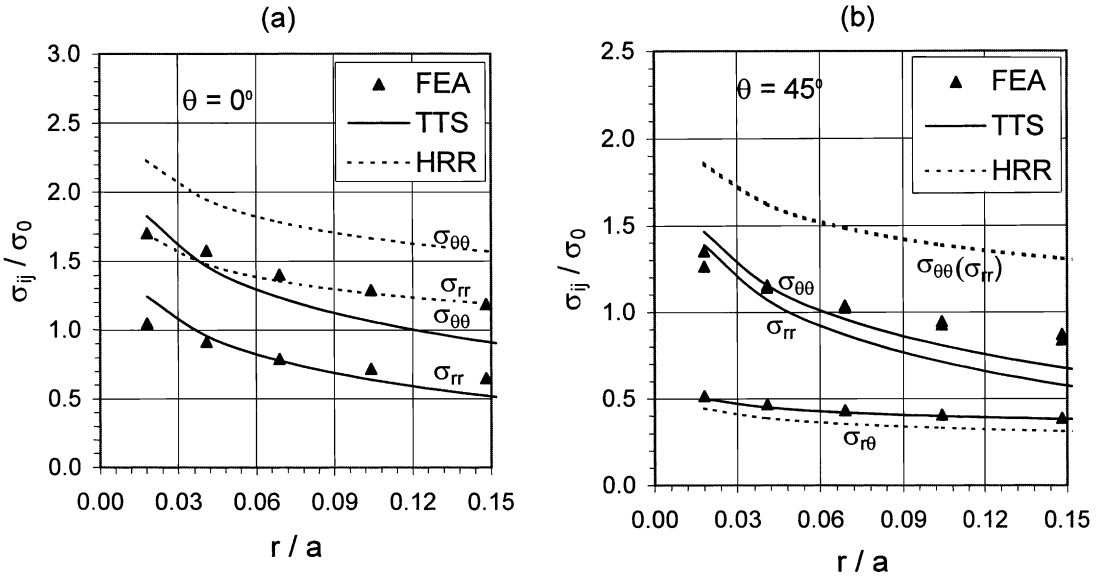

Fig. 10. Radial distributions of stresses at $t = 7.8t_T$ for SENT specimen with $a/W = 0.125$ (a) $\theta = 0°$ and (b) $\theta = 45°$.

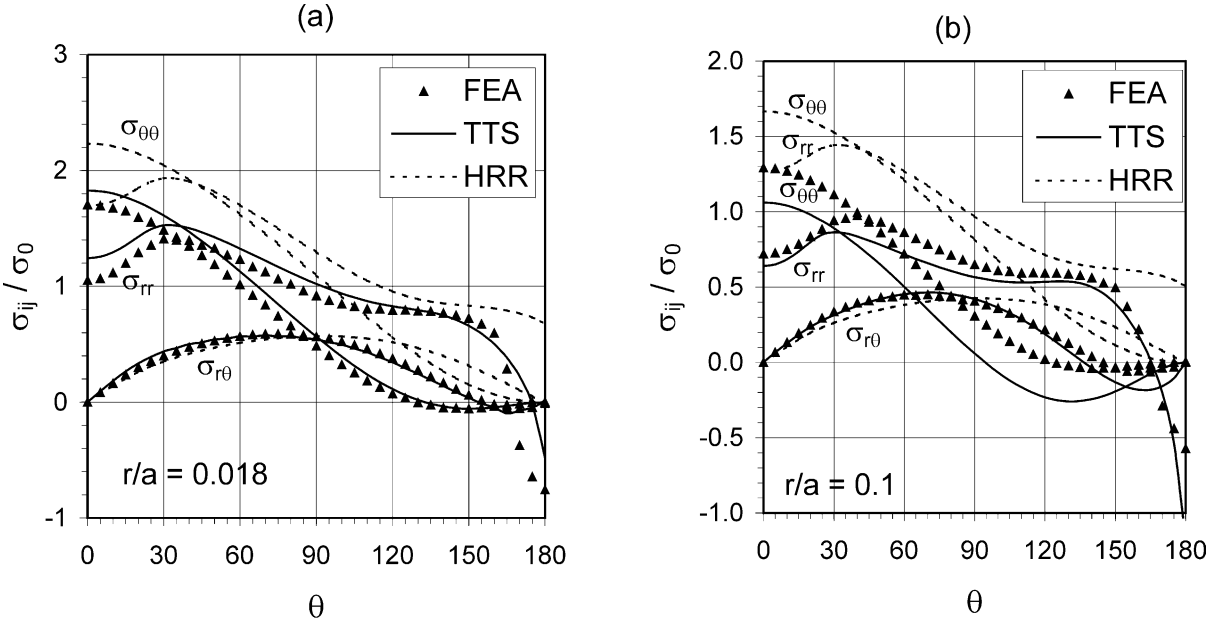

Fig. 11. Angular distributions of stresses at $t = 7.8t_T$ for SENT specimen with $a/W = 0.125$ (a) $r/a = 0.018$ and (b) $r/a = 0.1$.

both in the angular and the radial directions at least within $r/a \leqslant 0.1$. On the other hand, the HRR-type fields are far from the FEA results and the dominant zone of the HRR-type field is nearly non-existent. It is noted that $A_2 = -0.488$ was used in the presentation of the stresses shown in Figs. 6–11.

3.2.3. Time variation of stress field

Fig. 12 shows the temporal variations of stresses at a radial distance $r/a = 0.018$ in two different angular directions $\theta = 0°$ and $\theta = 45°$. It is found again that the three-term solutions match very well with FEA results near the crack tip for all the times considered here from $t = 0.1t_T$ to $t = 7.8t_T$. And, the HRR-type fields deviate from the FEA results for all the time except for the shear stress $\sigma_{r\theta}$. Moreover, the change of stress gradients with respect to the time is large when time $t \leqslant 0.8t_T$, and then is very small. At about $t = 4.0t_T$, the stress fields determined from the three-term solution and from the FEA calculations approach the steady-state stress field corresponding to the three-term solution (22) as shown in Fig. 12.

3.3. Single edge notched tension specimen with $a/W = 0.5$

A SENT specimen with a deep crack as illustrated in Fig. 1(a) is considered here. The specimen has a crack depth of $a/W = 0.5$, width $W = 1$ inch, length $2H = 8W$, and thickness $b = 1$ in. The remote uniform load is 4886 psi, which corresponds to an applied concentrated load of $P = 4886$ lb.

The results and analyses of Section 3.2.3 indicates clearly that the three-term solution (19) is universally valid for all times from the small-scale creep to the extensive creep. Moreover, the dominant zone of the three-term solution is nearly unaffected by the creep time when $t \geqslant t_T$. Therefore, hereafter, we only report and discuss results of stress fields at the transient time $t = t_T$ and focus our attention on the size of the dominant zone of the three-term solution.

For the SENT with $a/W = 0.5$, h_1 is equal to 0.928 from Kumar et al. (1981). From Eqs. (24) and (26), $t_T = 225.45$ h, $C^* = 0.008853$ psi-in/h. From FEA calculations, $C(t) = 0.0208$ psi-in/h at $t = t_T$, A_2 is determined as -0.556. Fig. 13(a) and (b) show the radial and angular variations of stress components σ_{rr}, $\sigma_{\theta\theta}$ and $\sigma_{r\theta}$ at $\theta = 0°$ and at $r/a = 0.09$ for the SENT specimen with a deep crack of $a/W = 0.5$. The radial distributions of stresses from the three-term solution at $\theta = 0°$ agree very well with the FEA results within $r/a \leqslant 0.2$ as shown in Fig. 13(a). All stress components from the three-term solution almost reproduce the

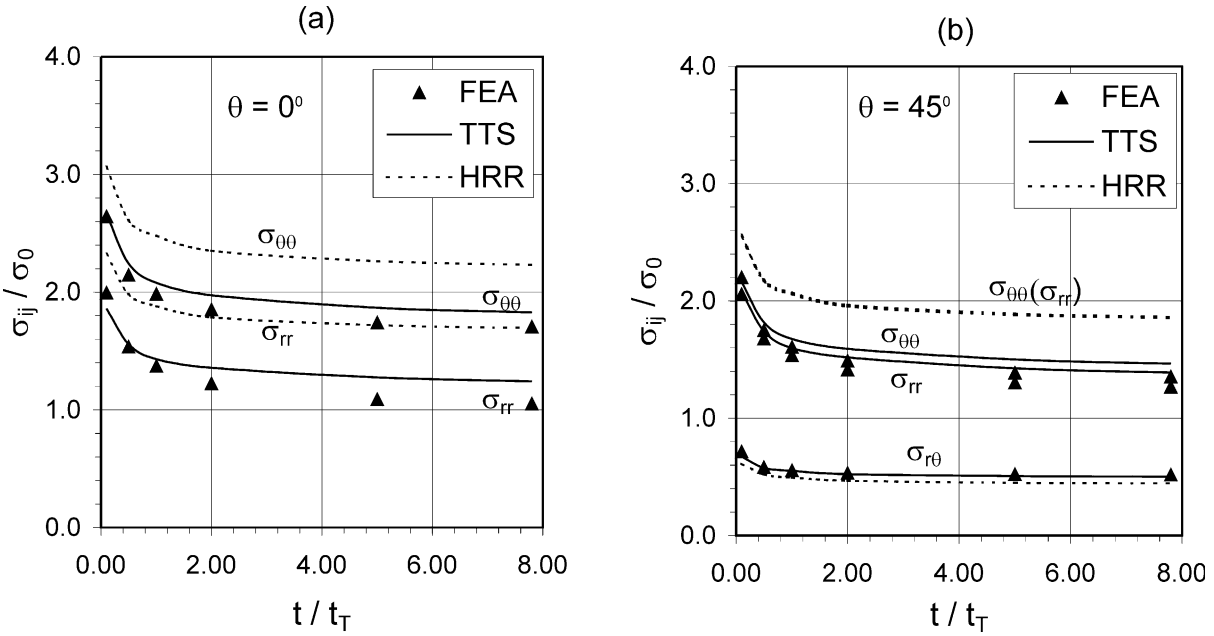

Fig. 12. Time variations of stresses for SENT specimen with $a/W = 0.125$ (a) $\theta = 0°$, $r/a = 0.018$ and (b) $\theta = 45°$, $r/a = 0.018$.

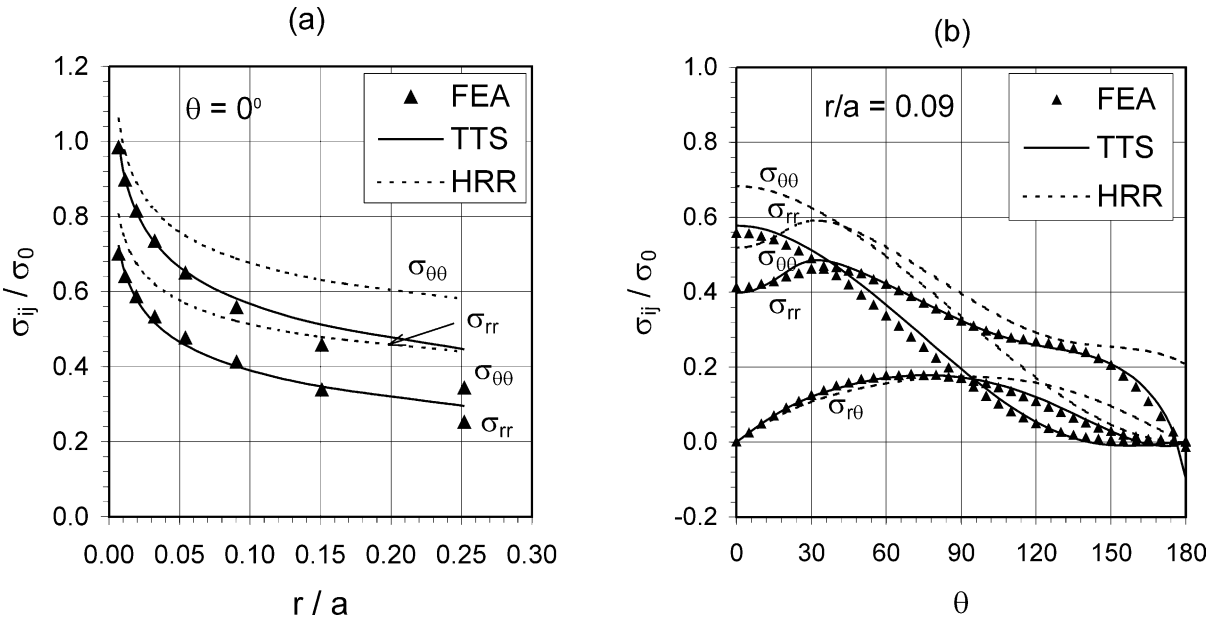

Fig. 13. Distributions of stresses at $t = t_T$ for SENT specimen with $a/W = 0.5$ (a) Radial distribution at $\theta = 0°$ and (b) Angular distribution at $r/a = 0.09$.

FEA results over the entire angular sectors at $r/a = 0.09$, as shown in Fig. 13(b). However, the HRR-type fields are far from the FEA results both in the radial and the angular directions. Relative to the shallow cracked SENT specimen, the three-term solutions for the deep cracked SENT match better with finite element results when compared at the same position from the crack tip.

3.4. Three-point bend, center-cracked panel, and compact tension specimens

This section reports results from the three-point bend (TPB), the center-cracked panel (CCP) and the compact tension (CT) specimens as shown in Fig. 1(b)–(d). TPB specimen has a crack depth of $a/W = 0.125$, span of $2H = 4W$. CCP specimen has a crack depth of $a/W = 0.125$, length of $2H = 4W$. CT specimen has a crack depth of $a/W = 0.25$, height of $2H = 1.2W$. The specimen width W (or half width for CCP) is 4 in. specimen thickness $b = 1$ in. for all three specimens. The applied load for TPB is 10 Klb, the tension load for CT is 12 Klb, and the remote uniform load for CCP is 18,750 psi which corresponds to a concentrated load of $P = 37.5$ Klb.

From the handbook (Kumar et al. (1981)), the C^*-integral expression (23) for the three specimens have the following forms:

(a) TPB specimens

$$C^* = B(W-a)h_1\left(\frac{P\sigma_0}{P_0}\right)^{n+1}, \tag{29}$$

where $h_1 = 0.687$ when $a/W = 0.125$, the reference load per unit thickness is

$$P_0 = \frac{1.455(W-a)^2\sigma_0}{2H}. \tag{30}$$

(b) CCP specimens

$$C^* = B(W-a)\frac{a}{W}h_1\left(\frac{P\sigma_0}{P_0}\right)^{n+1}, \tag{31}$$

where $h_1 = 4.35$ when $a/W = 0.125$, the reference load per unit thickness is

$$P_0 = \frac{4}{\sqrt{3}}(W-a)\sigma_0. \tag{32}$$

(c) CT specimens

$$C^* = B(W-a)h_1(P\sigma_0/P_0)^{n+1}, \tag{33}$$

where $h_1 = 1.48$ when $a/W = 0.25$, the reference load per unit thickness is

$$P_0 = 1.455\eta(W-a)\sigma_0 \tag{34}$$

in which

$$\eta = \sqrt{\left(\frac{2a}{W-a}\right)^2 + \frac{4a}{W-a} + 2} - \left(\frac{2a}{W-a} + 1\right). \tag{35}$$

From Eqs. (21), (29), (31) and (33), the transition time and C^*-integral can be obtained for the three specimens:

- For the TPB specimen, the transition time $t_T = 55.1$ h, $C^* = 0.08455$ psi-in/h. At time $t = t_T$, $C(t) = 0.1385$ psi-in/h from FEA. And the parameter $A_2 = -1.07$.
- For the CCP specimen, the transition time $t_T = 367.37$ h, $C^* = 0.001275$ psi-in/h. At time $t = t_T$, $C(t) = 0.00236$ psi-in/h from FEA. And the parameter $A_2 = -1.19$.
- For the CT specimen, the transition time $t_T = 40.78$ h, $C^* = 0.285$ psi-in/h. At time $t = t_T$, $C(t) = 0.352$ psi-in/h from FEA. And the parameter $A_2 = -0.2615$.

Fig. 14(a) and 14(b) show the radial and angular distributions of stress components σ_{rr}, $\sigma_{\theta\theta}$ and $\sigma_{r\theta}$ at $\theta = 0°$ and at $r/a = 0.05$ for the TPB specimen with $a/W = 0.125$. The radial distributions of the three-term solution at $\theta = 0°$ as shown in Fig. 14(a) agree well the FEA results only within $r/a \leqslant 0.0825$, and then deviate from the FEA results in a nearly linear variation. It indicates that the global bending stress impinges to the crack-tip stress field (c.f. Chao and Zhu, 1998; Zhu and Chao, 2000). The angular distribution of the three-term solution match very well with the FEA results over the entire angular sectors except for the region near the crack surface, as shown in Fig. 14(b). However, the HRR-type fields are far from the FEA results both in the radial and the angular directions.

Fig. 15 (a) and (b) show the radial and angular variations of stress components σ_{rr}, $\sigma_{\theta\theta}$ and $\sigma_{r\theta}$ at $\theta = 0°$ and at $r/a = 0.01$ for the CCP specimen with $a/W = 0.125$. The radial distributions of stresses at $\theta = 0°$ from the three-term solution agree very well with the FEA results within $r/a \leqslant 0.12$. The angular distributions of the three-term solution are in good agreement with the FEA results over the entire angular sectors except for the region near the crack surface. Again, the HRR-type fields deviate substantially from the FEA results both in the radial and the angular directions.

Fig. 16(a) and (b) show the radial and angular variations of stress components σ_{rr}, $\sigma_{\theta\theta}$ and $\sigma_{r\theta}$ at $\theta = 0°$ and at $r/a = 0.1$ for the CT specimen with $a/W = 0.25$. It is observed that the HHR-type field, the three-term solution and FEA results are very close to each other both in the radial and angular directions in this case. In the radial direction, the calculated stresses at $\theta = 0°$ are in good agreement with the HRR-type field

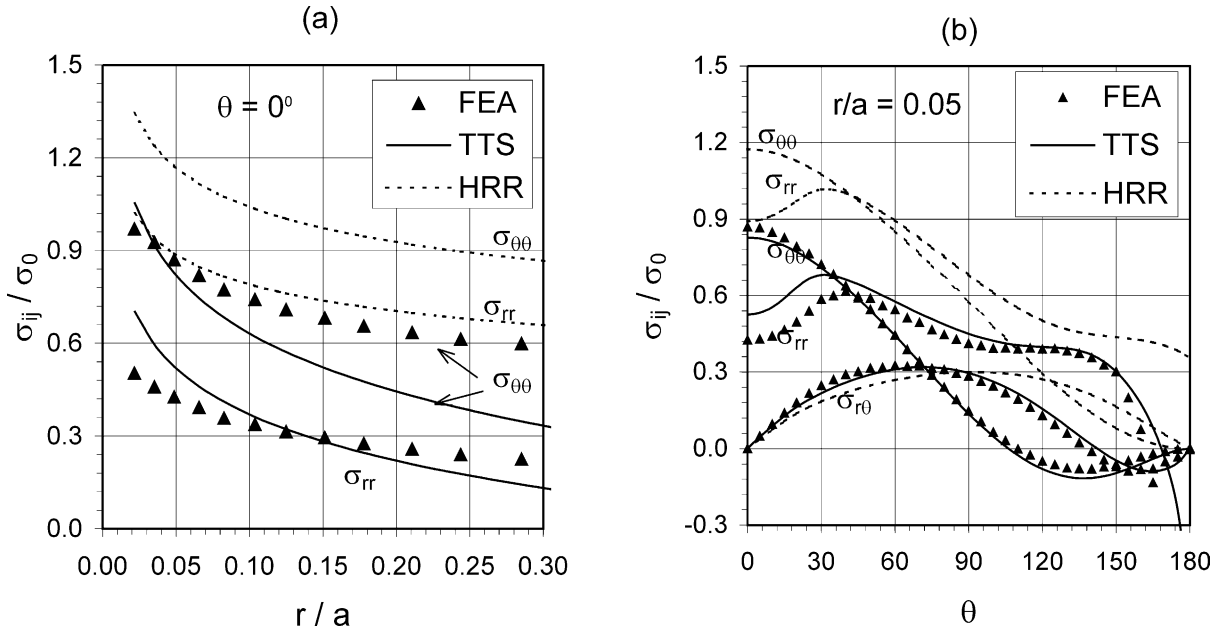

Fig. 14. Distributions of stresses at $t = t_T$ for TPB specimen with $a/W = 0.125$ (a) Radial distribution at $\theta = 0°$ and (b) Angular distribution at $r/a = 0.05$.

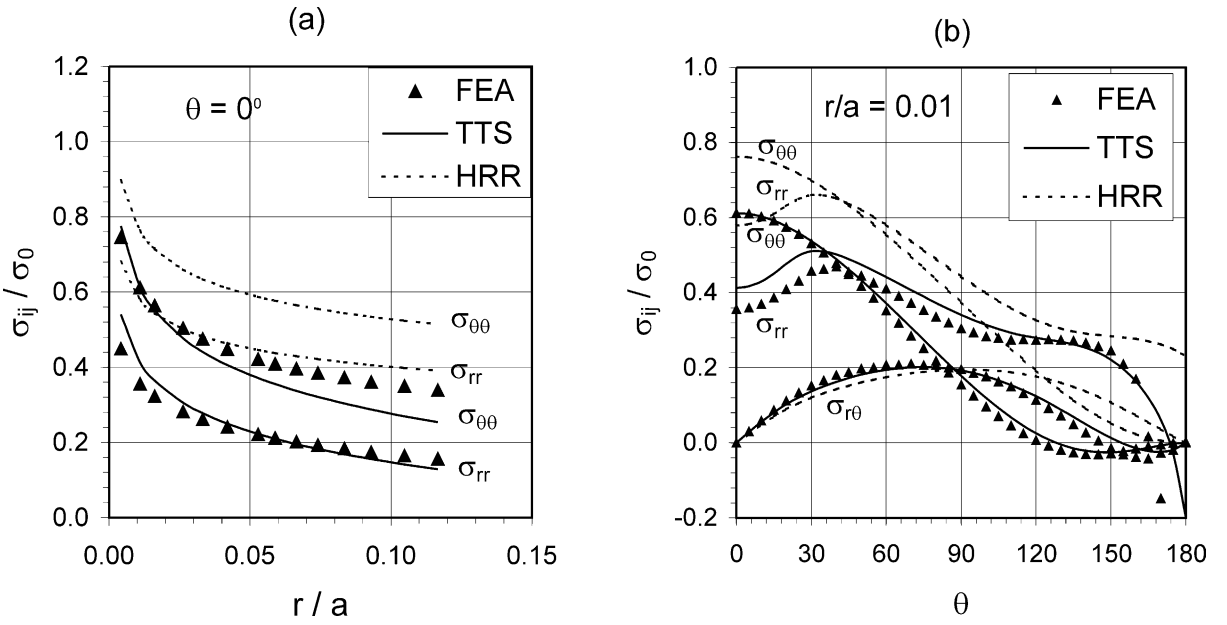

Fig. 15. Distributions of stresses at $t = t_T$ for CCP specimen with $a/W = 0.125$ (a) Radial distribution at $\theta = 0°$ and (b) Angular distribution at $r/a = 0.01$.

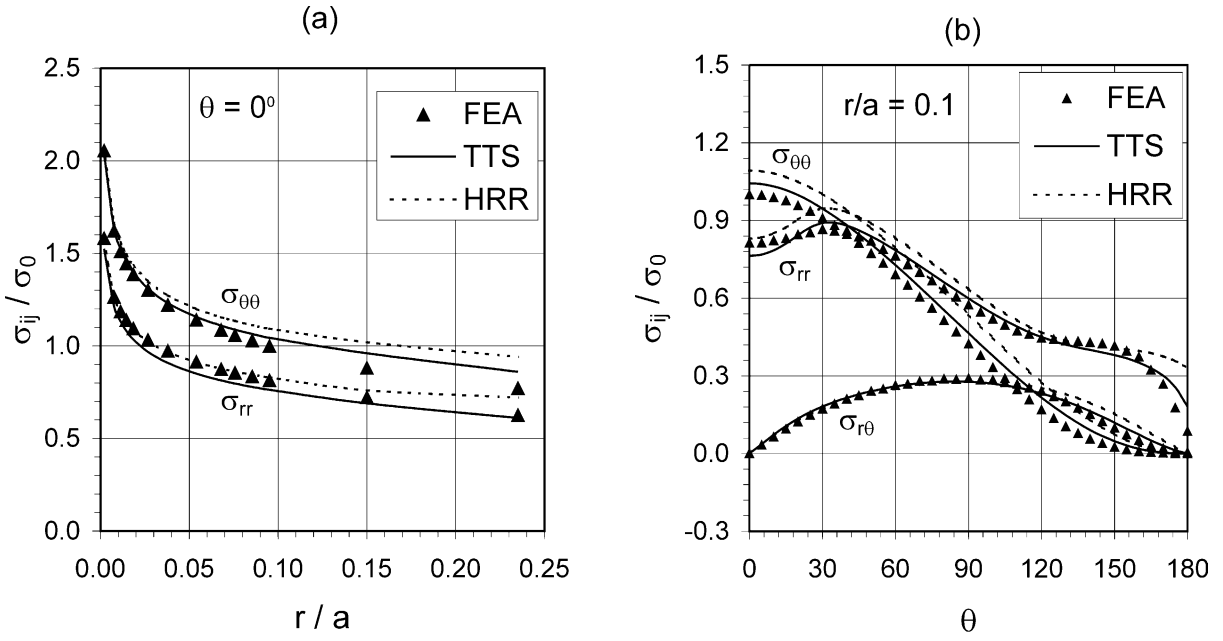

Fig. 16. Distributions of stresses at $t = t_T$ for CT specimen with $a/W = 0.25$ (a) Radial distribution at $\theta = 0°$ (b) Angular distribution at $r/a = 0.1$.

within $r/a < 0.1$, and with the three-term solution up to $r/a = 0.25$. Even at $r/a = 0.1$, the three-term solutions and the HRR-type fields are close to the FEA results as shown in Fig. 16(b) although the three-term solutions are slightly closer to the FEA results. Accordingly, it can be stated that for CT-specimen, the HRR type solution provides good characterization for the crack-tip fields and the three-term solution should replace the HRR-type field only at a distance further away from the crack tip.

4. Conclusions

The higher-order asymptotic crack-tip fields are investigated in the present paper for a mode-I crack in a creeping material under the plane strain conditions. Based on the three-term solution of Yang et al. (1993) and Chao et al. (1994) for hardening materials, this paper extends and develops a three-term solution near a crack tip in creeping materials with only two parameters: $C(t)$-integral and additional parameter $A_2(t)$. The asymptotic analysis reveals that all basic governing field equations for the elastic power-law creeping materials are the same as those given by Yang et al. (1993) or Nikishkov (1995a) for the elastic power-law hardening materials. Accordingly, the structure and property of the solutions are completely similar for the two types of materials. In addition, the following conclusions can be made:

(a) Except the amplitudes of the three-term asymptotic solution, i.e. $C(t)$ and $A_2(t)$, all stress exponents and the dimensionless angular functions of stresses, strain rates and displacement rates are same as those for power-law hardening materials and can be found in the report of Chao and Zhang (1997).

(b) The three-term solutions have only two independent parameters: $C(t)$-integral and additional parameter A_2. This additional parameter A_2 can be interpreted as a constraint parameter and is independent of the position from the crack tip. The first term solution is the HRR-type singularity field.

(c) For moderate to low creeping materials, i.e. the creep exponent $n \geqslant 3$, the $C(t)$–A_2 three-term solution is the pure creeping solution and the elastic strains do not play a role on the crack-tip fields.

(d) For the pure power-law materials or under extensive creep condition, the constraint parameter A_2 is independent of applied loading $C(t)$ and thus the creep time t.

To assess the validity of the three-term asymptotic solution, detailed FEA is performed for four typical specimens: SENT with a shallow crack of $a/W = 0.125$ and a deep crack of $a/W = 0.5$, TPB with a crack of $a/W = 0.125$, CCP with a crack of $a/W = 0.125$ and CT with a crack of $a/W = 0.25$. The extensive comparison indicates that the HRR-type field can only be used in the crack-tip fields with high constraints, such as the SENT specimens under small-scale creep and the CT specimens, and deviates substantially from the finite element results for all low constraint specimens. However, the $C(t)$–A_2 three-term solution compare well with the finite element results in both angular and radial distributions and dominate a crack-tip region of $r/a \leqslant 0.1$ at least for all specimens considered here. Therefore, it can be concluded that the three-term asymptotic solution developed in this work is a valid solution to characterize the crack-tip mechanics fields for specimens ranging from high constraints to low constraints and from small-scale creep to extensive creep. This conclusion is especially true for low constraint specimens, where the HRR-type field loses the dominant region.

Acknowledgements

The authors acknowledge the support from National Science Foundation through NSF/EPSCoR Co-operative Agreement EPS-9630167 and from US Air Force Office of Scientific Research (AFOSR).

References

Bassani, J.L., McClintock, F.A., 1981. Creep relaxation of stress around a crack tip. International Journal of Solids and Structures 17, 479–492.

Betegon, C., Hancock, J.W., 1991. Two parameter characterization of elastic–plastic crack-tip fields. Journal of Applied Mechanics 58, 104–110.

Chao, Y.J., Yang, S., Sutton, M.A., 1994. On the fracture of solids characterized by one or two parameters: theory and practice. Journal of Mechanics and Physics of Solids 42, 629–647.

Chao, Y.J., Zhang, L., 1997. Tables of Plane Strain Crack Tip Fields: HRR and Higher Order Terms, Me-report 97-1, Department of Mechanical Engineering, University of South Carolina.

Chao, Y.J., Zhu, X.K., 1998. J–A_2 characterization of crack-tip fields: extent of J–A_2 dominance and size requirements. International Journal of Fracture 89, 285–307.

Chao, Y.J., Zhu, X.K., 2000. Constraint-modified *J–R* curves and applications to predict ductile crack growth. International Journal of Fracture, in press.

Ehlers, R., Riedel, H., 1981. A finite element analysis of creep deformation in a specimen containing a macroscopic crack, Advances in Fracture Research, vol. 2, Proceedings of the Fifth International Conference on Fracture, Cannes, France, pp. 691–698.

Hoff, N.J., 1954. Quarterly of Applied Mechanics 12, 49–55.

Hutchinson, J.W., 1968. Singular behavior at the end of a tensile crack in a hardening material. Journal of Mechanics and Physics of Solids 16, 13–31.

Kumar, V., German, M.D., Shih, C.F., 1981. An Engineering Approach to Elastic–Plastic Analysis. EPRI NP-1931, Electric Power Research Institute, Palo Alto, CA.

Li, F.Z., Needlemen, A., Shih, C.F., 1988. Characterization of near tip stress and deformation fields in creeping solids. International Journal of Fracture 36, 163–186.

Nikishkov, G.P., 1995a. An algorithm and a computer program for the three-term asymptotic expansion of elastic–plastic crack-tip stress and displacement fields. Engineering Fracture Mechanics 50, 65–83.

Nikishkov, G.P., Bruckner-foit, A., Munz, D., 1995b. Calculation of the second fracture parameter for finite cracked bodies using a three-term elastic–plastic asymptotic expansion. Engineering Fracture Mechanics 52, 685–701.

Nortan, F.H., 1929. The Creep of Steel at High Temperatures. McGraw-Hill, New York.

O'Dowd, N.P., Shih, C.F., 1991. Family of crack-tip fields characterized by a triaxiality parameter – I: Structure of fields. Journal of the Mechanics of Physics and Solids 39, 989–1015.

Ohji, K., Ogura, K., Kubo, S., 1979. Stress–strain field and modified integral J-integral the vicinity of a crack tip under transient creep conditions. Japanese Society of Mechanical Engineer 790-13, 18–20 (in Japanese).

Riedel, H., 1981. Creep deformation at crack tip in elastic–viscoplastic solids. Journal of Mechanics and Physics of Solids 29, 35–49.

Riedel, H., Rice, J.R., 1980. Tensile cracks in creeping solids. Fracture Mechanics: Twelfth Conference, ASTM STP 700, American Society for Testing and Materials, pp. 112–130.

Rice, J.R., Rosengren, G.F., 1968. Plane strain deformation near a crack tip in a power-law hardening material. Journal of Mechanics and Physics of Solids 16, 1–12.

Sharma, S.M., Aravas, N., Zelman, M.C., 1995. Two-parameter characterization of crack tip fields in edge-cracked geometries: plasticity and creep solution. Fracture Mechanics: 25th Volume, ASTM STP 1220, American Society for Testing and Materials, Philadelphia, pp. 309–327.

Shih, C.F., 1983. Tables of Hutchinson-Rice-Rosengren singular field quantities. MRL E-147, Division of Engineering, Brown University.

Shih, C.F., O'Dowd, N.P., Kirk, M.T., 1993. A framework for quantifying crack tip constraint. Constraint Effects in Fracture, ASTM STP 1171, American Society for Testing and Materials, Philadelphia, pp. 2–20.

Yang, S., Chao, Y.J., Sutton, M.A., 1993. Higher order asymptotic fields in a power-law hardening material. Engineering Fracture Mechanics 45, 1–20.

Yang, L., Sutton, M.A., Deng, X., Lyons, J.S., 1996. Finite element analysis of creep fracture initiation in a model superalloy material. International Journal of Fracture 81, 299–320.

Zhu, X.K., Chao, Y.J., 1999. Characterization of constraint of fully plastic crack-tip fields in non-hardening materials by the three-term solution. International Journal of Solids and Structures 36, 4497–4517.

Zhu, X.K., Chao, Y.J., 2000. Fully plastic crack-tip fields for CCP and DECPP specimens under tension in non-hardening materials. International Journal of Solids and Structures 37, 577–589.